Biogeosciences Discuss., 11, 7235–7271, 2014
www.biogeosciences-discuss.net/11/7235/2014/
doi:10.5194/bgd-11-7235-2014

Biogeosciences Discussions
Open Access

Spatial variability and the fate of cesium in coastal sediments near Fukushima, Japan

E. Black and K. O. Buesseler

Woods Hole Oceanographic Institution, 266 Woods Hole Road, Mail Stop #25, Woods Hole, MA 02543-1050, USA

Received: 12 February 2014 – Accepted: 7 May 2014 – Published: 20 May 2014

Correspondence to: E. Black (eblack@whoi.edu) and K. O. Buesseler (kbuesseler@whoi.edu)

Published by Copernicus Publications on behalf of the European Geosciences Union.

Abstract

Quantifying the amount of cesium incorporated into marine sediments as a result of the Fukushima Dai-ichi Nuclear Power Plant (FDNPP) accident has proven challenging due to the limited multi-core sampling from within the 30 km zone around the facility, the inherent spatial heterogeneities in ocean sediments, and the potential for inventory fluctuations due to physical, biological, and chemical processes. Using ^{210}Pb, ^{234}Th, ^{137}Cs, and ^{134}Cs profiles from 20 sediment cores, coastal sediment inventories were reevaluated. A minimum ^{137}Cs sediment inventory of 100 ± 50 TBq was found for an area of 55 000 km^2 using cores from this study and a total of 130 ± 60 TBq using an additional 181 samples. These inventories represent less than 1 % of the estimated 15–30 PBq of cesium released during the FDNPP disaster and constitute ~ 90 % of the total coastal inventory of ^{137}Cs remaining in 2012. The time needed for surface sediment activities (0 to 3 cm) at the 20 locations to reduce by 50 % via bioturbation was estimated to range from 0.4 to 26 years, indicating a much greater persistence of cesium in the sediments relative to coastal water activities. However, due to the observed variability in mixing rates, grain size, and inventories, additional cores are needed to further improve estimates and capture the full extent of cesium penetration into the shallow coastal sediments, which was deeper than 14 cm for all cores retrieved from water depths less than 150 m.

1 Introduction

The Tohoku earthquake and tsunami of 11 March 2011 led to multiple system failures at the Fukushima Dai-ichi Nuclear Power Plant (FDNPP). Over the next month, cooling water releases and hydrogen explosions resulted in the largest nuclear disaster since Chernobyl. Oceanic inputs included direct cooling discharge, runoff, riverine flow, and an estimated 70 to 80 % of the total atmospheric radionuclide release (Aoyama et al., 2012). While later reports indicate additional releases to the ocean (TEPCO, 2014),

BGD
11, 7235–7271, 2014

the initial ^{137}Cs activities measured in the FDNPP discharge channel from March to May of 2011 represent the most significant oceanic contribution to date, peaking at 68 million Bq m^{-3} in April 2011 (Buesseler et al., 2011, 2012). ^{137}Cs emerged as the major oceanic contaminant warranting long-term study due to its ~ 30 year half-life and large release, generally estimated to be around 15–30 PBq (Buesseler, 2014; Charette et al., 2013; Chino et al., 2011; Stohl et al., 2011). ^{137}Cs and ^{134}Cs ($t1/2 \sim 2$ years) have been found with comparable activities near the FDNPP and were released with a ratio of ~ 1 (Buesseler et al., 2011). Although they are highly soluble in the coastal ocean (Buesseler et al., 2012), a small percentage of the release will have been incorporated into the marine sediments and may remain associated with the seafloor, even after currents transport much of the dissolved phase away from the coast. Initial studies of the sediments near the FDNPP have already shown the widespread incorporation of ^{137}Cs well above the relatively small remaining 1960's fallout signal of 1–2 Bq kg^{-1} (dry) (NRA, 2014b; Kusakabe et al., 2013; Otosaka and Kato, 2014; Otosaka and Kobayashi, 2013).

The most spatially and temporally extensive sediment datasets have been provided by the Ministry of Education, Culture, Sports, Science and Technology-Japan (MEXT) and the Tokyo Electric Power Company (TEPCO). TEPCO has reported some of the highest ^{134}Cs sediment activities (2000 Bq kg^{-1} wet; NRA, 2014a) in grab samples collected within the 30 km zone around FDNPP. However, lacking bulk density measurements, inventory estimates have not been published for this region. MEXT, on the other hand, reported monthly multi-corer, dry activities for homogenized 0 to 3 cm core tops from outside the 30 km zone (NRA, 2014b). Kusakabe et al. (2013) used 30 different MEXT locations ranging from 45 to 675 m water depth to estimate a ^{137}Cs sediment inventory of 38 TBq for the top 3 cm. As both datasets are limited to the uppermost layers of the sediment column, calculations using only these measurements will underestimate the total incorporation of cesium into the sediments. In a more recent effort, Otosaka and Kato (2014) paired MEXT cores with 10 cm Smith-McIntyre grab samples

BGD
11, 7235–7271, 2014

and sectioned cores ranging from 3 to 10 cm and estimated a ^{134}Cs coastal inventory of 200 ± 60 TBq, decay-corrected to March 2011.

Larger datasets are essential for more accurate sediment inventory calculations due to the spatial variability and local heterogeneity observed in previous coastal sediment studies from this region (Kusakabe et al., 2013; Thornton et al., 2013). Kusakabe et al. (2013) found a ^{137}Cs activity range of 170 to 580 Bq kg^{-1} with six successive multi-corer casts at nominally the same sampling site (mean and standard deviation of 330 ±160 Bq kg^{-1} dry). In addition, Thornton et al. (2013) reported activity fluctuations of < 10 to 1500 Bq kg^{-1} at sites located between 5 and 10 km of the FDNPP and from 500 to 40 000 Bq kg^{-1} within 3 km of the FDNPP. These local anomalies were observed over distances of less than 1 km using a continuous (1 hertz) towed gamma ray spectrometer and their magnitude illustrates the importance of high spatial resolution sampling.

The evolution and ultimate fate of cesium isotopes in the coastal ocean must be better constrained to assess both the short term implications of the FDNPP accident and the potential for lasting effects. Reports that bottom water fish contain higher cesium concentrations than pelagic fish suggest that the sediments could be a continued source to bottom-dwelling biota (Buesseler, 2012). A model study of the coastal food chain near Fukushima indicated that an additional contamination source beyond ocean water, mostly likely associated with the sediments, would be necessary to sustain the cesium levels observed in higher trophic organisms (Tateda et al., 2013). Although a few estimates of coastal inventories have been published (Kusakabe et al., 2013; Otosaka and Kato, 2014), the question of cesium's fate in the sediment reservoir remains open. Not only is there a lack of sufficient depth resolution within the sediment column to determine complete inventory estimates, but the potential for processes to alter the distribution of cesium in this reservoir, such as bioturbation, have only been approached qualitatively.

^{210}Pb ($t1/2 \sim 22.2$ years) and ^{234}Th ($t1/2 \sim 24$ days), naturally occurring daughter products in the ^{238}U decay series, can aid in evaluating the rates of sedimentation

BGD
11, 7235–7271, 2014

and bioturbation occurring in sediments from months to decades (Yang et al., 1985). ^{234}Th is particle reactive and will be scavenged easily in the upper ocean, leading to a potential excess in sediments ($^{234}Th_{ex}$). Because of its short half-life, measureable $^{234}Th_{ex}$ is generally only observed in the top few cm of the sediment column in areas of rapid and recent mixing. Excess ^{210}Pb ($^{210}Pb_{ex}$) is supplied via atmospheric deposition, from the decay of ^{222}Rn gas, and scavenging in the water column. In sediments $^{210}Pb_{ex}$ represents the divergence from secular equilibrium with ^{226}Ra (supported ^{210}Pb). If conditions are relatively stable, the $^{210}Pb_{ex}$ in a given area will represent the flux to this location averaged over the last century (~ 5 half-lives).

We estimated the expected sediment inventories of $^{210}Pb_{ex}$ in the coastal sediments near Fukushima, Japan using an average $^{210}Pb_{ex}$ atmospheric delivery flux of approximately 200 Bq m^{-2} yr^{-1} to obtain an inventory from atmospheric inputs of 6400 Bq m^{-2} (200 × 32 years, mean life of ^{210}Pb). The atmospheric delivery flux estimate was derived from average monthly ^{210}Pb deposition measurements from 1993 to 2001 for Tokai-Mura (Ueno et al., 2003) and from 2000 to 2001 for Tokyo and Sendai (Yamamoto et al., 2006). A rough scavenging flux for ^{210}Pb can be calculated using a Pacific ^{210}Pb/^{226}Ra ratio of 0.75 (Tsunogai and Harada, 1980) with a deep sea ^{226}Ra activity (28.5° N and 145° E; Nozaki and Tsunogai, 1976) of approximately 33 dpm per 100 kg. This flux would be a linear function of water depth over which the disequilibrium applies, and ranges from 70 to 7000 Bq m^{-2} for depths of 50 m to 5000 m (1-D scavenging supply equal to the product of (^{226}Ra-^{210}Pb) the decay constant λ, the water depth, and 32 years). Thus, in most coastal settings, the dominant supply of ^{210}Pb is atmospheric deposition, whereas inventories are expected to increase with depth in the shelf and slope due to scavenging processes in the water column above. In addition, with a relatively long residence time for scavenging, ocean margins in general are sites of enhanced boundary scavenging of ^{210}Pb (Cochran et al., 1990).

BGD
11, 7235–7271, 2014

2 Methods

2.1 Sample collection

Twenty sediment cores ranging in length from 6 to 20 cm were collected during cruise campaigns in May 2012 (R/V *Tansei Maru*), June and July 2012 (R/V *Mirai*), May 2013 (R/V *Umitaka Maru*), and September 2013 (R/V *Daisan Kaiyu Maru*). Stations were located 2 to 1865 km from the FDNPP (Supplement S1). Cores were retrieved with a multi-corer and cross-sectioned at sea into 0.5 to 2 cm layers. A sample (plug) of 1 or 7 cm^3 was taken from each layer as the cores were cross-sectioned for density calculations. Sediment layers were preserved in sealed bags and the plug samples in capped vials. Eight, homogenized 5 cm cores (R1 to R8) were retrieved from a single cast at the location of core 13 for an analysis of local variability.

2.2 Grain size analysis

Grain size analysis was performed on a subset of ~ 3 cm^3 core samples using a Beckman Coulter LS13320 particle size analyzer with capabilities of 0.4 µm to 2 mm. Grain size results are reported as percent clay and percent fines (silt plus clay) averaged over the entire depth of each core. Percent clay and percent fines were calculated by summing the frequency outputs from 0 to 3.86 µm and from 0 to 63.41 µm, respectively. D50 values were determined, which signify the grain size at which 50 % of the sample is smaller or larger by particle count. While the reported uncertainty of the Coulter counter was minimal, a 5 % uncertainty was assumed for all results due to sampler bias and potential variation within each layer. Samples from cores 15 and 16 consisted of up to 42 % of grains over 1 mm by mass and were processed differently due to the counter limitations. To ensure that no prolate grains with a near 2 mm axis passed to the counter, a 1 mm sieve was placed over the sample delivery system. The total mass of sample used, ranging from 5 to 45 grams, was determined by the counter's optimal obscuration range or percentage of light blockage by grains (15 to 25 %).

BGD
11, 7235–7271, 2014

2.3 Isotope measurements

The remaining samples were dried at 40–60 °C for a minimum of 1 day and analyzed using Canberra GCW4030S germanium gamma well detectors for the following energy peaks: 46.5 keV (^{210}Pb), 63.3 keV (^{234}Th), 352 keV (^{214}Pb), 661 keV (^{137}Cs), 795 keV (^{134}Cs). Samples were counted for 7 to 24 h depending on the time to achieve counting uncertainties of less than 5 % on the primary peaks. Detectors were calibrated using a dilute pitchblende ore standard (US EPA Environmental Monitoring Systems Lab) and river sediment standard (NBS 4350 B). Minimum detectable activities (MDAs) were calculated using 24 h background spectra and efficiencies based on the average sample mass of 16.75 grams and sample volume of 14.5 mL (Currie, 1968). The calculated MDAs in Bq kg^{-1} were 4.2 (^{210}Pb), 3.2 (^{234}Th), 0.7 (^{214}Pb), 0.4 (^{137}Cs), and 0.8 (^{134}Cs). Activities under the MDAs and those with counting uncertainties over 50 % were reported as not detectable (ND). Total uncertainties for a given sample and isotope (in Bq kg^{-1}) represent the higher of either the counting uncertainty or 7 %. The minimum uncertainty (7 %) is the average percent difference between sample activity results when duplicate measurements were made using the same and different detectors. The total uncertainty is propagated through all activity and inventory calculations for individual sections and full cores.

^{210}Pb activities were decay-corrected to the collection date and adjusted for supported values from ^{214}Pb (assumed to be at equilibrium with parent ^{226}Ra) to determine $^{210}Pb_{ex}$. Since an excess of ^{234}Th generally exists only in the first few cm, an estimation of equilibrium values at depth were used to determine $^{234}Th_{supported}$, the activity derived only from the decay of its ^{238}U parent, to calculate $^{234}Th_{ex}$ (decay-corrected to collection). All ^{134}Cs and ^{137}Cs data were decay-corrected to the date of maximum concentrations at the FDNPP (6 April 2011; Buesseler et al., 2011) unless noted. Over the timescale of our study ^{134}Cs was decaying, and thus by decay-correcting, the changes we observe can be attributed to physical and biological processes and not radioactive decay.

BGD
11, 7235–7271, 2014

Layer inventories in Bq m^{-2} were calculated for ^{134}Cs, ^{137}Cs, ^{210}Pb$_{ex}$, and ^{234}Th$_{ex}$ using the following relationship:

$$\text{Inventory} = \text{Layer Thickness} \times \text{Bulk Density} \times \text{Activity} \quad (1)$$

where layer thickness was in meters, activities were in Bq kg^{-1}, and bulk density (kg m^{-3}) was equal to the amount of dry mass of sample in the 1 or 7 cm^3 plug divided by the total volume. All layer inventories for each isotope were summed to calculate total inventories for each individual core except for ^{234}Th$_{ex}$, which was only reported for the exponentially decreasing surface activities. Because core depths ranged from 6 to 20 cm, some core inventories may not be representative of the complete isotope profile at that location, especially if ^{210}Pb$_{ex}$ values remain high at depth.

2.4 Modeling

While the mixing of marine sediments often occurs via spatially and temporally variable bioturbation processes, such as non-local transport, the cumulative result of sediment accumulation, mixing, and isotope decay is often modeled as a diffusive process and can be written

$$\frac{\partial}{\partial t}\{\rho(1-\phi)\times A\} = \frac{\partial}{\partial x}\left\{D_B\rho(1-\phi)\frac{\partial A}{\partial x}\right\} - \frac{\partial}{\partial x}\{\rho(1-\phi)w\times A\} + \rho(1-\phi)\lambda A \quad (2)$$

where ρ represents density, A activity of radionuclide, t time, w sedimentation rate, and λ represents the decay constant (Cochran, 1985). To generate mixing rates (D_B) using this relationship for each core, steady state, constant porosity (ϕ), and constant D_B with depth (x) were assumed within each selected profile region. Sedimentation was considered to be negligible over the decadal timescales considered. Equation (2) was simplified based on the above assumptions to form the following relationship (Cochran, 1985; Yang et al., 1985)

$$\text{Activity} = A_0 e^{-x\sqrt{\frac{\lambda}{D_B}}} \quad (3)$$

BGD
11, 7235–7271, 2014

where A_o is the activity at $x = 0$. A dynamic, exponential regression analysis was performed on $^{234}Th_{ex}$ and $^{210}Pb_{ex}$ activity (Bq kg^{-1}) profile sections of each core using Eq. (3). Surface D_B values were determined using $^{234}Th_{ex}$ when present. $^{210}Pb_{ex}$ was used to calculate mixing rates for continuous sections below the termination of $^{234}Th_{ex}$, generally starting from 1.5 to 3.0 cm.

We used the $^{210}Pb_{ex}$- and $^{234}Th_{ex}$-derived D_B values and the shallowest surface ^{137}Cs activities at each location to model the expected changes over time in ^{137}Cs profiles using a simple pulse equation (Cochran, 1985; Yang et al., 1985):

$$\frac{A}{A_o} = e^{\frac{-z^2}{4D_B t}} \quad (4)$$

where A is the activity at any given depth z, A_o is the shallowest surface activity, D_B is the mixing rate, and t is the time since the pulse maximum (6 April 2011; Buesseler et al., 2011). Keeping all other variables constant, we modeled the cesium activity profiles for varying dates, including those of other studies to assess the comparability of cores, and determined the time needed for average cesium activities from the top 3 cm to decrease by 50 % since the Fukushima pulse maximum due to bioturbation and hence, the mixing of the cesium pulse deeper into the core.

3 Results and discussion

3.1 Variability between multi-core tubes

From a single multi-corer cast, we retrieved 8 subcores (R1 to R8) and analyzed each for $^{210}Pb_{ex}$, ^{137}Cs, and ^{134}Cs. Core 13 was retrieved from the same location during an additional mutli-corer cast (Fig. 1). We observed ^{137}Cs activities in the 5 cm subcores that varied from 45 ± 3 to 220 ± 20 Bq kg^{-1} and a range of $^{210}Pb_{ex}$ activities from 140 ± 10 to 220 ± 20 Bq kg^{-1} (Supplement S2). Inventories for ^{137}Cs were 1600 ± 100

BGD
11, 7235–7271, 2014

to 6500 ± 500 Bq m^{-2} and 5500 ± 400 to 7800 ± 600 Bq m^{-2} for $^{210}Pb_{ex}$. Inventories for core 13 were even greater for cesium, with values of 8000 ± 200 and 6400 ± 200 Bq m^{-2} for ^{137}Cs and $^{210}Pb_{ex,}$ respectively. We could not obtain a coefficient of determination (R^2) greater than 0.1 for an exponential, logarithmic, or linear regression of ^{134}Cs and $^{210}Pb_{ex}$ inventories, which suggests that the factors controlling local inventories may vary for the two isotopes (Supplement S3). Overall, cesium had greater activity and inventory variability, even more so if core 13 was considered. The large differences observed between multi-core tubes of the same cast indicate that any one sediment core may not be representative of a region of seafloor, reiterating the need for spatially and temporally extensive datasets.

The replicate cores and core 13 produced comparable D50, percent fines, and percent clay results across all samples relative to the order of magnitude differences seen in cesium activities (Supplement S4). D50 values ranged from 19 to 41 µm, percent clay from 7.3 to 12, and percent fines from 66 to 85. Although a study of the Irish Sea found elevated ^{137}Cs activities with increasing percentages of higher surface area particles (Poole et al., 1997), such as clays, we could not recreate this trend with the replicate core data and could not find any relationship (exponential, linear, or logarithmic) with an R^2 value of greater than 0.1 between the three grain size parameters and cesium activities or inventories at this single site (Supplement S5). $^{210}Pb_{ex}$ activities showed some association with percent clay in the replicate cores (R^2 values ranging from 0.34 to 0.36). While Kusakabe et al. (2013) posited that low bulk densities could indicate finer grain sizes and abundant organic matter content, we did not see evidence of the former in the replicate cores. Although particle size characteristics may not control local differences in radionuclide activities where variations in size are comparatively minimal, they are important over larger regional scales (see Sect. 3.5).

BGD
11, 7235–7271, 2014

3.2 Zonal divisions

Previous studies have delineated various coastal regions for the purposes of sediment characterization and the estimation of total cesium delivery to the sediment reservoir near FDNPP. Kusakabe et al. (2013) used one boundary based on core locations from approximately 35.5° N to 38.5° S, while Otosaka and Kato (2014) used incremental isobaths running from 35.67° N to 38.50° S to create 8 separate zones (0 to 1500 m). For consistency, we used 35.5° N to 38.5° S for our northernmost and southernmost zonal boundaries and isobaths for eastern and western divisions (Fig. 1 and Table 1). We divided the sediment reservoir into five zones based on inventories, grain size, and mixing rate estimates from our 20 sediment cores (see Sects. 3.3 to 3.7). The northern coastal zone (NCZ, $n = 6$) and southern coastal zone (SCZ, $n = 3$) are bound by the 150 m isobath to the east. The northern and southern boundaries of the NCZ and SCZ were shortened to 38.20° N and 36.25° N, respectively, after consideration of additional surface cores from MEXT (Kusakabe et al., 2013) (see Sect. 3.9). The mid-coastal zone (MCZ, $n = 5$) is bound by the 800 m isobath to the east, and the Japanese coast, NCZ, and SCZ to the west. The offshore zone (OZ, $n = 4$) is bound to the west and east by the 800 m and 4000 m isobaths, respectively. Although retrieved from 4066 m, we included core 3 in the OZ because of its proximity to core 4 and an under representation of deeper cores in this zone. The remaining cores ($n = 2$) are located in the abyssal zone (AZ). All result and calculations in the following sections will be discussed relative to these zones.

3.3 Grain size analysis

Two cores from the OZ and all cores from the NCZ, SCZ, and MZ were analyzed by layer with a Beckman Coulter counter and the results were averaged by core (Table 1). The remaining 4 cores were visually assessed. The NCZ cores contained the lowest percent clay (0.2–0.8) and yielded the highest D50 values, ranging from 164 to greater than 690 µm. These cores had the lowest average standard deviations and were com-

BGD
11, 7235–7271, 2014

posed of relatively well-sorted sands. The SCZ cores contained more poorly sorted grain assemblages and could be characterized as mostly silt-dominated with some fine sands. D50 values for these cores ranged from 31 to 76 µm and the percent clay ranged from 4.9 to 8.8, an order of magnitude lower and higher than the NCZ cores, respectively. The MCZ cores were fairly similar in characteristics to the SCZ cores and ranged in percent clay from 5.2 to 9.9 and in D50 from 38 to 104 µm. The two OZ cores were very fine-grained and had relatively similar D50 and percent clay values of approximately 18 µm and 12.5 %, respectively.

The D50, percent fines, and percent clay results reflected wide variations in grain size over the coastal to offshore regions and relatively consistent vertical distributions within each core. We saw that as water depth increased to 5900 m, average grain sizes generally transitioned from coarser sands and granules (0.5 to 4 mm) to very fine silts and clays (< 63 µm). This broad relationship did not always hold true in the near-shore, however, as the NCZ and SCZ cores differed in average grain size characteristics but not in water depth. D50 values remained fairly consistent layer to layer within most cores. A few cores showed D50 layer variations up to 220 µm over 2 cm increments, but no observable pattern existed when these fluctuations were compared with changes in isotope activities. Conversely, many large layer to layer cesium fluctuations, like those seen in core 17, could not be explained by changes in grain size. Despite the likelihood that some or all of the cores might contain tsunami deposits, there was no grain size evidence of fining-upward sequences in these cores, sharp layer contacts with largely differing grain sizes, or definitive indicators that would allow us to separate potential tsunami layers from sections impacted by bio-irrigation, bioturbation, or local physical processes (Sakuna et al., 2012).

3.4 Cesium activity profiles

Average surface activities (top 3 cm) in the 20 cores ranged from 2.1 ± 0.1 to 640 ± 40 Bq kg^{-1} for ^{137}Cs and from 0 to 550 ± 30 Bq kg^{-1} for ^{134}Cs (Supplement S6). The AZ cores contained no detectable ^{134}Cs. The OZ sediment activities ranged from 0 to

BGD
11, 7235–7271, 2014

$13 \pm 1\,\mathrm{Bq\,kg^{-1}}$ for ^{134}Cs, while the MCZ activities ranged from 2.7 ± 0.5 to $57 \pm 3\,\mathrm{Bq\,kg^{-1}}$ for ^{134}Cs. NCZ cores 15 through 19 had a similar, albeit lower, average surface activity ($28\,\mathrm{Bq\,kg^{-1}}$) than that of the 5 MCZ cores ($36\,\mathrm{Bq\,kg^{-1}}$). While these NCZ cores had unexpectedly low ^{134}Cs activities, due to their proximity to the FDNPP, core 20, located within 3 km of the FDNPP, contained an average of $550 \pm 30\,\mathrm{Bq\,kg^{-1}}$ in the top 3 cm. With the exception of this single core in the NCZ, the cores in the SCZ had the highest activities of all zones, with ^{134}Cs values ranging from 167 ± 7 to $230 \pm 10\,\mathrm{Bq\,kg^{-1}}$.

Full-core cesium profiles varied strongly in shape and penetration depth between zones (Fig. 2). Cores in the AZ and OZ had either fallout-only profiles with no ^{134}Cs and very low ^{137}Cs or rapidly decreasing ^{134}Cs and ^{137}Cs activities with depth. FDNPP-derived cesium penetration was limited to the top 3 cm in these zones. The MCZ cores generally showed similar exponentially decreasing activities with depth with the exception of core 11, which showed a pronounced cesium peak between 1 and 4 cm. The penetration depth of ^{134}Cs was deeper here, on average, than in the AZ and OZ cores. The SCZ cores maintained substantially higher cesium activities from 0 to 8 cm relative to most other cores and we observed both exponential curves and vertical profiles below 8 cm. Penetration depths for ^{134}Cs were at least 16 cm in the SCZ. While the NCZ cores had similar surface activities to those in the MCZ, most cores in this zone showed distinctive semi-vertical profiles from the surface to the coring depths. Core 17 was the only exception and the only core to exhibit activity large fluctuations with depth. Because we observed ^{134}Cs at all core bottoms and without decreasing trends in most of the NCZ cores, we could not estimate penetration depths beyond our sampling intervals.

3.5 Cesium inventories

Total ^{134}Cs and ^{137}Cs inventories ranged from 0 to $74\,000 \pm 2000\,\mathrm{Bq\,m^{-2}}$ and 21 ± 1 to $73\,000 \pm 2000\,\mathrm{Bq\,m^{-2}}$, respectively (Table 1). Our inventory range for ^{137}Cs was almost four times larger than those reported in Kusakabe et al. (approximately 100

BGD
11, 7235–7271, 2014

to 18 000 Bq m^{-2}; 2013) and Otosaka and Kato (approximately 100 to 19 100 Bq m^{-2}; 2014). This could be attributed to both greater core lengths and larger total area sampled, including the 30 km zone around the FDNPP. Inventories generally decreased with water depth. AZ and OZ inventories were less than 400 Bq m^{-2} for both isotopes and the MCZ contained only one core inventory above 1000 Bq m^{-2}. Excluding core 20, we observed cesium inventories on the order of 1500 to 7000 Bq m^{-2} in the NCZ and 4000 to 36 500 Bq m^{-2} in the SCZ. The cesium inventories for core 20 were double that of the next highest value and clearly reflected a proximity to the FDNPP. Pre-accident cores from the broader western north Pacific have been reported to contain 10 s to 1000 s of Bq m^{-2} of ^{137}Cs (Moon et al., 2003; Lee et al., 2005). Assuming a weapons testing delivery of 2500 Bq m^{-2} for 30° to 40° N (Bowen et al., 1980) and 1–5 % delivery to the sediments, we expect an average sediment inventory of less than 50 Bq m^{-2} prior to Fukushima. We observed inventories consistent with weapons testing fallout in the AZ and OZ cores (^{134}Cs/^{137}Cs of 0 to 0.86). Larger inventories and ^{134}Cs/^{137}Cs ratios of ~ 1 in most of the MCZ, NCZ, and SCZ cores suggested negligible contributions from weapons testing ^{137}Cs.

Since many prior studies have focused on the 0 to 3 cm surface layer, we also calculated the percentage of total inventory that lay below 3 cm within each of our cores (Table 1). Percentages generally increased with shallower water depths. We observed 75 ± 6 % and 75 ± 5 % for ^{134}Cs and 73 ± 7 % and 75 ± 5 % for ^{137}Cs (mean ± std. dev.) below 3 cm as a fraction of the total inventory in the NCZ and SCZ, respectively. The percentages for those cores in the MCZ ranged from 0 to 33 % for ^{134}Cs and from 10 to 36 % for ^{137}Cs. The average inventory below 3 cm in the MCZ cores attributed to Fukushima (^{134}Cs) was 15 ± 16 %, which agreed closely with the Otosaka and Kato (2014) ^{134}Cs average from this zone of 19 %. When we combined the two datasets for this zone (n = 15) the average inventory below 3 cm was 18 ± 16 %. In the OZ we saw no ^{134}Cs below 3 cm in any of the cores and a range of 0 to 32 % for ^{137}Cs. We did not observe any inventories of either isotope below 3 cm in the AZ.

BGD
11, 7235–7271, 2014

The core inventories from this study reflect changes in three main factors: distance from the FDNPP, water depth, and grain size. Proximity clearly impacted core 20, located within 3 km of the FDNPP (Fig. 3a). Figure 3a, shows a general decrease in inventories with increasing distance from the FDNPP and water depth, despite that the remaining core inventories show little to no statistical relationship to proximity or water depth (exponential regression R^2 values of 0.06 and 0.24). Grain size was a controlling factor in the near-shore NCZ and SCZ, where cores were sampled from similar water depth ranges and yet contained widely varying inventories (Table 1, Fig. 3a). Although no trend was observed at the local scale between similar magnitude grain sizes and cesium activities in our one-cast replicate analysis, the larger differences in grain size between the SCZ and NCZ (D50 s from ~ 30 to 700 µm) corresponded to changes in total ^{134}Cs inventories. The NCZ and SCZ grain size trends mimic those observed in the Irish Sea, where an estimated 41 PBq of cesium released over 40 years preferentially incorporated into an area known as the Sellafield mud patch (Poole et al., 1997). In summary, proximity dominated within the 3 km zone of FDNPP, despite the sand content of core 20 (D50 of 164 µm, percent sand ~ 94 %), grain size was most important in the NCZ and SCZ, where initial water column activities were most likely the highest, and water depth and delivery mechanisms may have contributed to a greater extent in locations such as the MCZ and OZ, where water column activities were relatively low.

3.6 $^{210}Pb_{ex}$ and $^{234}Th_{ex}$ activities and inventories

$^{210}Pb_{ex}$ surface activities ranged from 12 ± 3 to 2000 ± 100 Bq kg^{-1} and generally increased with water depth, as expected, due to the increased input from water column scavenging (Supplement S6, Figs. 1 and 2). $^{210}Pb_{ex}$ activities were lowest in the NCZ and highest in the AZ. Intra-zonal $^{210}Pb_{ex}$ activity ranges were smaller than for cesium. Similar to the vertical cesium activity profiles observed in the NCZ, those of $^{210}Pb_{ex}$ remained relatively constant with depth. In the other zones, activities generally decreased with core depth, but also exhibited a variety of profile shapes. Generally, the

BGD
11, 7235–7271, 2014

termination of $^{210}Pb_{ex}$, the depth where all ^{210}Pb is supported, was not attained within our sampling depths, with the exception of cores 3 and 6 (Fig. 2).

$^{210}Pb_{ex}$ inventories, ranging from 2700±200 to 28 000±1000 Bq m^{-2}, reflect changes in grain size, water depth and local processes, and give support to the similar trends observed for cesium inventories (Table 1, Figs. 1 and 3b). $^{210}Pb_{ex}$ inventories generally increased with water depth. The NCZ values were slightly lower than anticipated (average inventory of 4100 Bq m^{-2}) based on our expected atmospheric inventory calculation of 6400 Bq m^{-2} and the SCZ values were more than twice as high as expected (average inventory 18 800 Bq m^{-2}). The SCZ zone is therefore a likely deposition center, receiving additional fine particles via horizontal transport. These trends are supported by the prevalence of sands in the NCZ cores and higher percentages in the SCZ cores of fines, similar to that observed with cesium inventories (He and Walling, 1996). An exponential regression of $^{210}Pb_{ex}$ inventories vs. percent clay indicated a strong relationship ($R^2 > 0.9$) between grain size and inventories. The MCZ, OZ, and AZ core inventories of $^{210}Pb_{ex}$ were generally one to four times higher than atmospheric delivery. This finding is similar to along the shelf and slope of the northeast USA (Buesseler et al., 1985/1986) and can be attributed to both scavenging within the water column, which is higher with increasing water depth, and horizontal transport and faster scavenging rates over boundary sediments in general. Evidence of boundary scavenging of ^{210}Pb has been shown for the NW Pacific by Cochran et al. (1990) based upon an analysis of deep sediment cores and the expected inventories from water column scavenging and atmospheric sources.

Of the 17 cores that were analyzed rapidly enough to measure $^{234}Th_{ex}$, 15 contained $^{234}Th_{ex}$ activities, ranging from 20±10 to 1300±100 Bq kg^{-1} in the top 0 to 0.5 cm. Surface (0 to 3 cm) $^{234}Th_{ex}$ inventories peaked at 2400±300 Bq m^{-2} in the SCZ. Most cores showed classic exponential $^{234}Th_{ex}$ profile shapes with higher values at the surface that dropped to near zero excess values within 1 to 3 cm. Although the lowest $^{234}Th_{ex}$ inventories were found in the OZ and NCZ and the highest were generally located in the

BGD
11, 7235–7271, 2014

SCZ and MCZ, intra-zonal variability was high and more often than not inventories did not vary negatively with increasing depth.

3.7 Bioturbation estimates

Since all of the cores showed evidence of bioturbation, we attempted to approximate local mixing rates using $^{234}Th_{ex}$ and $^{210}Pb_{ex}$ activity profiles with a steady-state diffusive mixing model (Eq. (3), see Fig. 4 for example profile). Mixing rates in the MCZ, OZ, and AZ ranged from 0.7 to 9.6 $cm^2\,yr^{-1}$ for $^{234}Th_{ex}$-derived estimates and from 0.06 to 3.7 $cm^2\,yr^{-1}$ for $^{210}Pb_{ex}$-derived estimates (Table 2). At a given location, $^{234}Th_{ex}$-derived estimates were generally higher as they reflect processes occurring in the uppermost active sediment layers (Aller and Cochran, 1976). Mixing rates in the SCZ and NCZ reflected intense bioturbation, with full core $^{210}Pb_{ex}$-derived estimates starting at 11 $cm^2\,yr^{-1}$ and the majority of rates being unquantifiable due to the vertical $^{210}Pb_{ex}$ profiles. The wide range in rates was not unexpected with cores from diverse sedimentary environments and water depths. While $^{234}Th_{ex}$-derived mixing rates were not correlated with water depth ($R^2 < 0.1$) we observed an exponentially decreasing trend in $^{210}Pb_{ex}$-derived mixing rates with water depth ($R^2 = 0.96$), as observed in other coastal regions where biomass, species diversity, and bioturbation decrease with depth (Henderson et al., 1999; Joydas and Damodaran, 2009).

Although $^{234}Th_{ex}$ was absent from some of the deepest AZ, OZ, and MCZ cores, we succeeded in obtaining $^{210}Pb_{ex}$ and $^{234}Th_{ex}$ mixing rates for most cores located in these zones. In general, the activity profiles exponentially decreased with depth (Figs. 2 and 4) and the AZ and OZ $^{210}Pb_{ex}$-derived mixing rates agreed well with the observed historical rates from this region of 0.1 to 1 $cm^2\,yr^{-1}$ (Moon et al., 2003; Yang et al., 1985). Cores from the shallowest regions (NCZ and SCZ) were the most difficult to fit with the bioturbation model. The SCZ cores generally contained 3 layers of mixing: a 1 to 3 cm moderately fast mixing zone at the surface, a 5 to 10 cm rapid mixing layer with an almost vertical profile, and a deep mixing zone with similar bioturbation rates as the

BGD
11, 7235–7271, 2014

surface layers. Equation (3) could not be used at all to derive $^{210}Pb_{ex}$ mixing rates for any of the NCZ cores due to the almost vertical activity profiles throughout. In these instances, the observed profile trends could have resulted from extremely rapid mixing or from resuspension and deposition resulting from a tsunami or storm-related event although we did not see evidence of individual storm deposits in the grain size analysis (see Sect. 3.3).

3.8 Cesium modeling of changes in surface activities

We were interested in predicting how quickly bioturbation would reduce surface (0 to 3 cm) cesium activities over time. To do this we calculated the change in surface cesium activity profiles since the Fukushima maximum at each core location, assuming a pulse-like input (Eq. 4). The $^{234}Th_{ex}$-derived mixing rate was used for the depths specified in Table 2 and the corresponding $^{210}Pb_{ex}$-derived mixing rate was used for the rest of the core. If no rate existed for one of the isotopes, the mixing rate from the other was applied to all depths. The decay of ^{137}Cs, although small over 5 to 10 years was subtracted from the profile activities after all other calculations. In general, the measured cesium activity profiles for the top 3 cm matched fairly well with the pulse model output for our sampling dates using the local bioturbation rate. Below 3 cm, the model generally followed the AZ, OZ, and MCZ measured cesium profiles (see Fig. 4 for example profile) and underestimated the NCZ and SCZ profiles.

The time from the Fukushima maximum until the surface (0 to 3 cm) activities decreased by 50 % ranged from 0.4 to 26 years for the 20 cores (Table 2). The SCZ times ranged from 0.4 to 0.9 years and the MCZ times from 2 to 15 years. We could not model any of the cesium profiles in the NCZ using $^{210}Pb_{ex}$ mixing rates and the two with $^{234}Th_{ex}$ mixing rates yielded estimates from 12 to 14 years, which is unrealistically long when the considering the water depth, vertical profiles, and the times calculated for the NCZ cores. The longest period for decrease in surface activities will occur in the slow-mixing OZ and AZ, whose 50 % reduction time varied from 6 to 26 years. Although

BGD
11, 7235–7271, 2014

these deep water locations may take at least two decades to decrease their 0 to 3 cm activities by 50 % due to bioturbation, the activities are much lower relative to the SCZ, which will change rapidly but started at activities 1 to 2 orders of magnitude higher.

3.9 Total seafloor cesium inventory calculations

We estimated that the marine sediments contained 100 ± 50 TBq of ^{137}Cs, at a minimum, for an area of approximately 55 000 km^2 (Table 3a and b). Because of the inventory variability and grain size influence in the NCZ and SCZ, the final totals for each zone were calculated by finding the mean inventory of all cores within that zone and multiplying by the area of the zone. Zonal and final totals are reported with standard deviations (Table 3b). Inventory calculations should represent underestimates of actual reservoir totals because the profiles in the highest inventory zones, the NCZ and SCZ, still showed Fukushima ^{134}Cs in their deepest sample layers. We did not calculate an inventory value for the AZ, which is extensive, but should not significantly contribute to overall inventories due to low cesium activities. Furthermore, our deepest cores, 1 and 2, did not contain Fukushima ^{134}Cs, although it has been detected in sediments as far as the Japan Trench (water depth of > 7000 m; Oguri et al., 2013).

To improve our inventory estimate, we used cores recovered in February 2012 by MEXT (Kusakabe et al., 2013) and those from August to November 2011 reported in Otosaka and Kato (2014) (OTKA). These datasets provided an additional 50 locations with either surface cores from recent sampling dates similar to this study's (MEXT) or cores with sufficient sampling depths to capture most to all of the cesium penetration into the local sediments (OTKA). The inventories of the shorter sediment cores were increased using the average percent ^{134}Cs inventory below 3 and 10 cm determined for each zone when applicable (see Sect. 3.5). Cesium activity and inventory values from the MEXT and OTKA datasets were not changed if the depth sampled was sufficient to capture the full extent of cesium penetration. The addition of 50 locations slightly increased the sediment inventory estimate to 100 ± 40 TBq, but did not substantially change the distribution of cesium between zones (Table 3a and b).

BGD
11, 7235–7271, 2014

In a final effort to further improve our inventory estimates, we utilized additional sampling dates from the 30 MEXT locations in Fig. 4 and calculated a total sediment reservoir estimate of 130 ± 60 TBq (n = 199) using the MEXT data from late June 2011 to February 2012 (Table 3b). The 30 locations were sampled at approximately monthly intervals. As we have observed, the range in local variability can be almost as high as that on the zonal or regional scale (Kusakabe et al., 2013; Thornton et al., 2013) so additional sampling at one site should not bias the zonal averages towards these repeated locations. Because mixing effects would be more significant in the top 3 cm, potentially moving cesium to deeper layers between MEXT's June 2011 sampling and our last sampling date in September 2013, we considered the sensitivity of our inventory estimate to rapid mixing. After adjusting for mixing, the total inventory estimate only decreased to 100 ± 60 TBq.

The three approximation methods all resulted in similar total ^{137}Cs sediment inventories, ranging from 100 to 130 TBq (Table 3a and b). The OZ comprised more than half the entire area but consistently totaled only 4 to 6 % of the ^{137}Cs sediment inventory. The MCZ contained between 15 and 18 % of the total ^{137}Cs in each case and made up 30 % of the total area. The NCZ was split into two subzones to account for the extremely high inventory observed within the 3 km radius of the FDNPP. Based on Thornton et al.'s continuous tow data, the area immediately around the nuclear facility (~ 3 km) showed the largest number of high ^{137}Cs Bq kg^{-1} anomalies relative to adjacent sediments (Thornton et al., 2013). Core 20 confirmed that this region was distinctly higher in activity and warranted its own subzone, so as not to skew the NCZ inventory average. The 3 km subzone adjacent to the FDNPP accounted for approximately 1 % of the total inventory. This inventory could change with the addition of new and deeper cores. However, with only 0.03 % of the total area, the addition should not change the total regional inventory substantially. The NCZ and the SCZ, on the other hand, contributed the most cesium by far (over 70 %), composed 9 % and 6 % of the total area, respectively, and consistently showed the greatest variability in inventories (Table 3a and b).

BGD
11, 7235–7271, 2014

Figures 5 and 6 show the spatial distribution of cesium inventories for all zones surrounding the FDNPP and illustrate both the high intra-zonal variability and the overall decrease of inventories with depth. Included are cores from this study (n = 18), from the February 2012 MEXT sampling dates (n = 30; Kusakabe, 2013), and from all OTKA dates (n = 20; Otosaka and Kato, 2014), the latter two containing adjusted cesium inventories when applicable (see Sect. 3.5). Best fit exponential regressions of these inventories vs. water depth are shown in Fig. 6. As observed with the cores from this study, the complied inventories from 0 to 150 m in the NCZ and SCZ had a low R^2 value (< 0.01) relative to water depth, which we suggest reflects the importance of grain size distribution in these zones (Fig. 3a). The compiled inventories from 150 to 1500 m showed a stronger relationship to water depth (R^2 = 0.3), although in any given region inventories still fluctuated by an order of magnitude.

4 Conclusions

Our ^{137}Cs marine sediment inventory estimates of approximately 100 to 130 TBq for 55 000 km^3 (0 to 4000 m water depth) represent the most comprehensive attempt to date for quantifying FDNPP cesium incorporation into the marine sediments. The coastal sediments contain the majority of the total TBq delivered, with inventories ranging from 100 to 125 TBq for 24 100 km^2 (0 to 800 m water depth). With expanded spatial coverage inside the 30 km radius of the FDNPP and improved vertical resolution in the NCZ and SCZ, our coastal inventory estimates fall between Kusakabe et al.'s (2013) 38 TBq and Otosaka and Kato's (2014) 200 TBq. Kusakabe et al. (2013) had calculated only surface inventories for the upper 3 cm for a similar area, thus providing a lower limit for total coastal inventories. Otosaka and Kato's (2014) estimate of 200 TBq is higher because it was calculated using exponential water depth vs. cesium inventory relationships that were derived without any NCZ cores, which effectively applied the relatively elevated SCZ core inventories to the entire NCZ and SCZ (Fig. 5).

BGD
11, 7235–7271, 2014

Our zonal analysis of cesium inventories, in conjunction with $^{210}Pb_{ex}$ and grain size analyses, has provided a robust estimate of the total cesium inventory that will inform future coring and towing efforts. We have identified key areas where more cores may improve inventory estimates. First, additional sampling is needed to supplement sparse coverage in two regions: north of the FDNPP along the coast, from 37.70° N to 38.20° N in the MCZ, and in locations deeper than 2000 m in the OZ. With the large observed spatial variability from scales of 1 m^2 (between multi-corer tubes) to 10 000 m^2 (among zones) greater numbers of cores are essential to give better constrain our estimates at present. Second, while most MCZ and OZ cores are long enough to capture complete cesium inventories, the cores in the NCZ and SCZ indicate that cesium had penetrated deeper than 18 to 20 cm. We have no means of predicting deeper profile shapes for these cores where we observed constant activity profiles for both $^{210}Pb_{ex}$ and the cesium isotopes. More extensive and deeper coring in both zones is needed to determine ultimate penetration depths and full inventories.

Both the relative inventories in the coastal environment and estimated zonal "recovery" timescales have implications for bottom-dwelling biota and those that may consume demersal species. If we assume a total ^{137}Cs release to the ocean of approximately 15 to 30 PBq from the Fukushima accident (Buesseler, 2014), our calculated sedimentary inventories comprise only less than 1.0 % of the total release in 2011. Only 15 TBq remain in coastal waters (Buesseler, 2014) and the sediment reservoir therefore currently represents approximately 86 to 90 % of the total ^{137}Cs inventory (water and sediment) off the coast of Japan. Water column inventories have continued to decrease since the accident, which makes the coastal sediments the most important long term reservoir of cesium isotopes. Rapid mixing in some locations may help to decrease overall biological access to these high activity sediments by transporting cesium isotopes deeper and therefore decreasing the overall activity of the more easily resuspended surface layers. While the MCZ and OZ require more time to reduce surface activities by 50 %, they do not pose as much of an environmental hazard because of their relatively low initial activities. The areas of greatest concern are the coastal zones

BGD
11, 7235–7271, 2014

shallower than 150 m water depth. Additional biological studies should take note of these zonal hotspots as cesium levels may remain elevated here much longer despite faster observed bioturbation rates.

In addition to bioturbation, other processes impacting cesium distributions in the coastal ocean require further study. Yamashiki et al. (2014) found that suspended particle loads in the Abukuma River Basin near Fukushima delivered over 5 TBq of cesium to the NCZ in a 10 month period. A typhoon that occurred during this time contributed more than half of this inventory over only 8 days. While 5 TBq would account for only 4 to 5 % of the total sediment reservoir, depending on where and how the particles are transported this contribution could create local hot spots. Chemical remobilization rates have not been published for this area of Japan, but are most likely less than 0.1 TBq per month for cesium, based on previous studies of the Irish Sea (Mitchell et al.,1999), and could decrease the total coastal inventory. Even though these contributions and losses are relatively small compared to the total cesium inventory of the sediments, only long term monitoring within the study region will indicate whether decay alone or other factors are controlling cesium activities and distributions over the next decade.

The Supplement related to this article is available online at doi:10.5194/bgd-11-7235-2014-supplement.

Acknowledgements. The authors would like to thank the captain, crew, and scientists aboard the R/V *Tunsei Maru*, R/V *Mirai*, R/V *Umitaka Maru*, and the R/V *Daisan Kaiyu Maru*. In particular, our samples were made possible by Jota Kanda, Jun Nishikawa, Makio Honda, and Shigeyoshi Otosaka. Field and laboratory assistance was provided by Crystal Brier, Stephanie Madsen, Chris Griner, and Steven Pike. The authors would also like to acknowledge the support of the Gordon and Betty Moore Foundation, Deerbrook Charitable Trust, Woods Hole Oceanographic Institution, and Massachusetts Institute of Technology.

BGD
11, 7235–7271, 2014

References

Aller, R. C. and Cochran, J. K.: $^{234}Th/^{238}U$ disequilibrium in near-shore sediment: particle reworking and diagenetic time scales, Earth Planet. Sc. Lett., 29, 37–60, 1976.

Aoyama, M., Tsumune, D., and Hamajima, Y.: Budgets and temporal change of radiocaesium distribution released from Fukushima NPP accidents in the North Pacific Ocean, Ocean Sciences Meeting, Salt Lake City, Utah, 21 February 2012, Session 88, 2012.

Bowen, V. T., Noshkin, V. E., Livingston, H. D., and Volchok, H. L.: Fallout radionuclides in the Pacific Ocean: vertical and horiztonal distributions, largely from GEOSECS stations, Earth Planet. Sc. Lett., 49, 411–434, 1980.

Buesseler, K. O.: Fishing for answers off Fukushima, Science, 338, 480–482, 2012.

Buesseler, K. O.: Fukushima and ocean radioactivity, Oceanography, 27, 1–13, 2014.

Buesseler, K. O., Livingston, H., and Sholkovitz, E.: $^{239,240}Pu$ and excess ^{210}Pb inventories alon gthe shelf and slope of the northeast USA, Earth Planet. Sc. Lett., 76, 10–22, 1985/1986.

Buesseler, K. O., Aoyama, M., and Fukasawa, M.: Impacts of the Fukushima Nuclear Power Plants on marine radioactivity, Environ. Sci. Technol., 45, 9931–9935, 2011.

Buesseler, K. O., Jayne, S. R., Fisher, N. S., Rypina, I. I., Baumann, H., Baumann, Z., Breier, C. F., Douglass, E. M., George, J., Macdonald, A. M., Miyamoto, H., Nishikawa, J., Pike, S. M., and Yoshida, S.: Fukushima-derived radionuclides in the ocean and biota off Japan, P. Natl. Acad. Sci. USA, 109, 5984–5988, 2012.

Charette, M. A., Breier, C. F., Henderson, P. B., Pike, S. M., Rypina, I. I., Jayne, S. R., and Buesseler, K. O.: Radium-based estimates of cesium isotope transport and total direct ocean discharges from the Fukushima Nuclear Power Plant accident, Biogeosciences, 10, 2159–2167, doi:10.5194/bg-10-2159-2013, 2013.

Chino, M., Nakayama, H., Nagai, H., Terada, H., Katada, G., and Yamazawa, H.: Preliminary estimation of release amounts of ^{131}I and ^{137}Cs accidentally discharged from the Fukushima Daiichi Nuclear Power Plant into the atmosphere, J. Nucl. Sci. Technol., 48, 1129–1134, 2011.

Cochran, J. K.: Particle mixing rates in the sediments of the eastern equatorial Pacific: evidence from ^{210}Pb, $^{239,240}Pu$ and ^{137}Cs distributions at MANOP sites, Geochim. Cosmochim. Ac., 49, 1195–1210, 1985.

BGD
11, 7235–7271, 2014

Cochran, J. K., McKibbin-Vaughan, T., Dornblaser, M. M., Hirschberg, D., Livingston, H. D., and Buesseler, K. O.: ^{210}Pb scavenging in the North Atlantic and North Pacific Oceans, Earth Planet. Sc. Lett., 97, 332–352, 1990.

Currie, L. A.: Limits for qualitative detection and quantitative determination, Anal. Chem., 40, 586–593, 1968.

He, Q. and Walling, D. E.: Interpreting particle size effects in the adsorption of ^{137}Cs and unsupported ^{210}Pb by mineral soils and sediments, J. Environ. Radioactiv., 30, 117–137, 1996.

Henderson, G. M., Lindsay, F. N., and Slowey, N. C.: Variation in bioturbation with water depth on marine slopes: a study on the Little Bahamas Bank, Mar. Geol., 160, 105–118, 1999.

Joydas, T. V. and Damodaran, R.: Infaunal macrobenthos along the shelf waters of the west coast of India, Arabian Sea, Indian J. Mar. Sci., 38, 191–204, 2009.

Kusakabe, M., Oikawa, S., Takata, H., and Misonoo, J.: Spatiotemporal distributions of Fukushima-derived radionuclides in nearby marine surface sediments, Biogeosciences, 10, 5019–5030, doi:10.5194/bg-10-5019-2013, 2013.

Lee, S. H., Povinec, P. P., Wyse, E., Pham, M. K., Hong, G. H., Chung, C. S., Kim, S. H., and Lee, H. J.: Distribution and inventories of ^{90}Sr, ^{137}Cs, ^{241}Am and Pu isotopes in sediments of the Northwest Pacific Ocean, Mar. Geol., 216, 249–263, 2005.

Mitchell, P. I., Condren, O. M., Vintró, L. L., and McMahon, C. A.: Trends in plutonium, americium and radiocaesium accumulation and long-term bioavailability in the western Irish Sea mud basin, J. Environ. Radioactiv., 44, 223–251, 1999.

Moon, D., Hong, G., Kim, Y., Baskaran, M., Chung, C. S., Kim, S. H., Lee, H., Lee, S., and Povine, P. P.: Accumulation of anthropogenic and natural radionuclides in bottom sediments of the Northwest Pacific Ocean, Deep-Sea Res. Pt. II, 50, 2649–2673, 2003.

Nozaki, Y. and Tsunogai, S.: ^{226}Ra, ^{210}Pb and ^{210}Po disequilibria in the western North Pacific, Earth Planet. Sc. Lett., 32, 313–321, 1976.

Nuclear Regulation Authority of Japan (NRA): Readings of Sea Area Monitoring in Marine Soil, available at: http://radioactivity.nsr.go.jp/en/list/247/list-1.html (last access: 10 February 2014), 2014a.

Nuclear Regulation Authority of Japan (NRA): Readings of Sea Area Monitoring in Sea Area by MEXT, available at: http://radioactivity.nsr.go.jp/en/list/260/list-1.html (last access: 10 February 2014), 2014b.

BGD
11, 7235–7271, 2014

Oguri, K., Kawamura, K., Sakaguchi, A., Toyofuku, T., Kasaya, T., Murayama, M., Fujikura, K., Glud, R. N., and Kitazato, H.: Hadal disturbance in the Japan Trench induced by the 2011 Tohoku-Oki earthquake, Scientific Reports, 3, 1915, doi:10.1038/srep01915, 2013.

Otosaka, S. and Kato, Y.: Radiocesium derived from the Fukushima Daiichi Nuclear Power Plant accident in seabed sediments: initial deposition and inventories, Environ. Sci. Process. Impacts, 16, 978–990, doi:10.1039/c4em00016a, 2014.

Otosaka, S. and Kobayashi, T.: Sedimentation and remobilization of radiocesium in the coastal area of Ibaraki, 70 km south of the Fukushima Dai-ichi Nuclear Power Plant, Environ. Monit. Assess., 185, 5419–5433, 2013.

Poole, A. J., Denoon, D. C., and Woodhead, D. S., The distribution and inventory of ^{137}Cs in sub-tidal sediments of the Irish Sea, in: Radioprotection: Radionuclides in the Ocean Les Editions de Physique, France, 32, edited by: Germain, P., Guary, J. C., Gueguenait, P., and Metivier, H., 422 pp., 1997.

Sakuna, D., Szczucinski, W., Feldens, P., Schwarzer, K., and Khokiattiwong, S.: Sedimentary deposits left by the 2004 Indian Ocean tsunami on the inner continental shelf offshore of Khao Lak, Andaman Sea (Thailand), Earth Planets Space, 64, 931–943, 2012.

Stohl, A., Seibert, P., Wotawa, G., Arnold, D., Burkhart, J. F., Eckhardt, S., Tapia, C., Vargas, A., and Yasunari, T. J.: Xenon-133 and caesium-137 releases into the atmosphere from the Fukushima Dai-ichi nuclear power plant: determination of the source term, atmospheric dispersion, and deposition, Atmos. Chem. Phys., 12, 2313–2343, doi:10.5194/acp-12-2313-2012, 2012.

Tateda, Y., Tsumune, D., and Tsubono, T.: Simulation of radioactive cesium transfer in the southern Fukushima coastal biota using a dynamic food chain transfer model, J. Environ. Radioactiv., 124, 1–12, 2013.

Tokyo Electric Power Company (TEPCO): Measures for Water Leakage, available at: http://www.tepco.co.jp/en/nu/fukushima-np/water/index-e.html (last access: 10 February 2014), 2014.

Thornton, B., Ohnishi, S., Ura, T., Odano, N., Sasaki, S., Fujita, T., Watanabe, T., Nakata, K., Ono, T., and Ambe, D.: Distribution of local ^{137}Cs anomalies on the seafloor near the Fukushima Dai-ichi Nuclear Power Plant, Mar. Pollut. Bull., 74, 344–350, 2013.

Tsunogai, S. and Harada, K.: ^{226}Ra and ^{210}Pb in the western North Pacific, in: Isotope Marine Chemistry, edited by: Goldberg, E. D., Horibe, Y., and Saruhashi, K., Uchida Rokakuho Publishing Company, Tokyo, 165–191, 1980.

BGD
11, 7235–7271, 2014

Ueno, T., Nagao, S., and Yamazawa, H.: Atmospheric deposition of ^{7}Be, ^{40}K, ^{137}Cs and ^{210}Pb during 1993–2001 at Tokai-mura, Japan, J. Radioanal. Nucl. Ch., 255, 335–339, 2003.

Yamamoto, M., Sakaguchi, A., Sasaki, K., Hirose, K., Igarashi, Y., and Kim, C. K.: Seasonal and spatial variation of atmospheric ^{210}Pb and ^{7}Be deposition: features of the Japan Sea side of Japan, J. Environ. Radioactiv., 86, 110–131, 2006.

Yamashiki, Y., Onda, Y., Smith, H. G., Blake, W. H., Wakahara, T., Igarashi, Y., Matsuura, Y., and Yoshimura, K.: Initial flux of sediment-associated radiocesium to the ocean from the largest river impacted by Fukushima Daiichi Nuclear Power Plant, Scientific Reports, 4, 3714, doi:10.1038/srep03714, 2014.

Yang, H.-S., Nozaki, Y., Sakai, H., Nagaya, Y., and Nakamura, K., Natural and man-made radionuclide distributions in Northwest Pacific deep-sea sediments: rates of sedimentation, bioturbation and ^{226}Ra migration, Geochem. J., 20, 29–40, 1985.

BGD
11, 7235–7271, 2014

Table 1. Grain size results and isotope inventories for sediment cores by zone. A general size was assigned to cores 1, 2, 3, and 5 after visual inspection, as grain size analysis was not possible for these cores. All other cores are described according to the Udden–Wentworth scale with sediment classifications, C (clay), M (silt), and S (sand), and size qualifiers vf (very fine), f (fine), m (medium), c (coarse), and vc (very coarse). The uncertainty on all inventory values represents the propagation of the counting uncertainty for each section (minimum 7 %) as discussed in Sect. 2.3. [a] Grain size results for cores 15 and 16 represent the fraction of sediment passed through a 1 mm sieve, 68 % of the total sample mass for C15 and 89 % for C16. Total D50 for these samples would be higher than the reported values and the percent clay and percent silt plus clay would be lower. The extra mass cannot be accounted for in the table values because the grain size analyzer measures by counts. ND = Not Detectable, – = not analyzed. [b] Decay-corrected to FDNPP discharge maximum.

Zone	No.	Water Depth (m)	D50 (μm)	% Clay (< 4 μm)	% Silt and Clay (< 63.4 μm)	Udden-Wentworth Classification	$^{210}Pb_{ex}$ (Bq m^{-2})	$^{234}Th_{ex}$ (Bq m^{-2})	^{134}Cs (Bq m^{-2})[b]	^{137}Cs (Bq m^{-2})[b]	% ^{134}Cs Inventory Below 3 cm	% ^{137}Cs Inventory Below 3 cm
Abyssal	1	5900	–	–	–	M	28 000 ± 1000	–	ND	84 ± 3	ND	0
	2	5156	–	–	–	M	19 500 ± 700	–	ND	26 ± 1	ND	0
Offshore	3	4066	–	–	–	M	4800 ± 200	50 ± 30	ND	21 ± 1	ND	0
	4	3259	18	12	87	C to vfS	22 500 ± 600	320 ± 60	32 ± 5	73 ± 4	0	32 ± 3
	5	1300	–	–	–	M	15 400 ± 500	–	190 ± 10	220 ± 10	0	13 ± 1
	6	1260	18	13	79	C to fS	16 800 ± 500	1700 ± 100	280 ± 20	370 ± 10	0	3 ± 0
Mid-Coastal	7	546	38	9.9	68	vfM to fS	7900 ± 200	1100 ± 100	55 ± 8	97 ± 4	0	29 ± 2
	8	497	49	6.8	62	vfM to fS	16 100 ± 400	2300 ± 100	870 ± 20	850 ± 20	33 ± 2	36 ± 2
	9	321	43	7.2	65	vfM to fS	13 400 ± 300	800 ± 100	540 ± 30	540 ± 20	13 ± 1	21 ± 1
	10	309	100	5.2	42	fM to mS	14 600 ± 400	1000 ± 100	840 ± 30	840 ± 20	0	10 ± 1
	11	205	100	6.8	46	vfM to mS	12 200 ± 400	1500 ± 100	3200 ± 100	2900 ± 100	30 ± 1	32 ± 1
Southern Coastal	12	125	31	8.7	68	vfM to fS	19 200 ± 400	1500 ± 100	4400 ± 100	3800 ± 100	73 ± 4	72 ± 3
	13	125	39	8.8	66	vfM to fS	19 700 ± 400	810 ± 80	13 700 ± 300	12 600 ± 300	69 ± 3	67 ± 3
	14	65	76	4.9	42	vfM to fS	17 400 ± 400	2400 ± 300	36 500 ± 800	30 300 ± 600	82 ± 3	81 ± 3
Northern Coastal	15	120	690[a]	0.3[a]	1.7[a]	mS to vcS	3800 ± 200	200 ± 100	1800 ± 100	1650 ± 40	69 ± 5	69 ± 3
	16	60	540[a]	0.2[a]	1.1[a]	mS to vcS	4600 ± 200	310 ± 40	2900 ± 100	2900 ± 100	77 ± 3	79 ± 3
	17	35	340	0.6	4.2	fS to cS	6600 ± 200	600 ± 100	6800 ± 100	5800 ± 100	83 ± 4	82 ± 3
	18	35	240	0.2	0.8	fS to cS	2700 ± 200	ND	6700 ± 100	6500 ± 100	76 ± 3	76 ± 3
	19	23	550	0.2	1.1	mS to cS	3300 ± 200	650 ± 80	5700 ± 100	5400 ± 100	75 ± 4	76 ± 4
	20	14	160	0.8	5.7	vfS to mS	3600 ± 200	ND	74 000 ± 2000	73 000 ± 2000	73 ± 5	69 ± 4

BGD
11, 7235–7271, 2014

Table 2. Mixing rates and model results for sediment cores. NP = Not Possible because no $^{234}Th_{ex}$ present or insufficient trends in $^{234}Th_{ex}$ or $^{210}Pb_{ex}$[1]. Due to the limited number of surface $^{234}Th_{ex}$ points, the uncertainties reported represent the higher of the standard uncertainty of the model fit for variable D_B or 25 % of D_B. [2] Values represent the time in years since the Fukushima maximum for surface concentrations (0–3 cm) to decrease by 50 % via mixing (modeled). The uncertainties reflect the mixing rate(s) used in the model.

Zone	No.	$^{234}Th_{ex}$-Derived D_B ($cm^2\ yr^{-1}$)[1]	Depths Used (cm)	$^{210}Pb_{ex}$-Derived D_B ($cm^2\ yr^{-1}$)	Depths Used (cm)	Estimated Years Until 50 % Decrease in Surface Cesiu m^2
Abyssal	1	NP		0.06 ± 0.02	1.5–5	26 ± 2
	2	NP		0.6 ± 0.2	1.5–9	10 ± 2
Offshore	3	NP		0.07 ± 0.02	0.5–3	26 ± 2
	4	0.8 ± 0.2	0–2	NP		6 ± 2
	5	NP		0.5 ± 0.1	1.5–9	11 ± 2
	6	5.5 ± 4	0–1.5	0.09 ± 0.02	2–8	24 ± 1
Mid-Coastal	7	0.9 ± 0.7	0–3	0.8 ± 0.2	2–8	5 ± 2
	8	2.4 ± 0.6	0–2	0.3 ± 0.1	1.5–5	15 ± 1
	9	0.7 ± 0.2	0–2	0.8 ± 0.1	2–8	8 ± 1
	10	9.6 ± 3	0–2	3.7 ± 0.4	3–8	2 ± 1
	11	1.6 ± 0.4	0–1.5	0.6 ± 0.1	1.5–10	10 ± 1
Southern Coastal	12	2.7 ± 0.7	0–1.5	12 ± 2	1.5–20	0.8 ± 0.2
	13	NP		11 ± 2	0–19	0.9 ± 0.2
	14	2.5 ± 0.6	0–2	22 ± 6	2–16	0.4 ± 0.2
Northern Coastal	15	0.3 ± 0.1	0–2	NP		14 ± 2
	16	0.4 ± 0.1	0–2	NP		12 ± 4
	17	NP		NP		NP
	18	NP		NP		NP
	19	NP		NP		NP
	20	NP		NP		NP

BGD
11, 7235–7271, 2014

Table 3a. Zonal statistics used for inventory estimates. Cores from group (1) are from this study only. Samples in group (2) were taken from Otasaka and Kato (2014; OTKA). Group (3) includes MEXT cores from February 2012 only and group (4) contains MEXT cores from (3) plus additional cores from the end of June 2011 through February 2012 (Kusakabe et al., 2013).

	Zone	Depth Ranges (m)	Area (km^2)	% of Area	No. of Sample Points (1) This Study	(2) OTKA	(3) MEXT	(4) MEXT
OZ		800–4000	30 832	56 %	4	3	0	0
MCZ		150–800	16 087	29 %	5	10	17	77
SCZ		0–150	3,309	6 %	3	7	7	43
NCZ	Greater Area	0–150	4,731	9 %	5	0	6	41
	3 km radius		14	0.03 %	1	0	0	0
	Total	0–4000	54 973 km^2		18	20	30	161

BGD
11, 7235–7271, 2014

Table 3b. Total ^{137}Cs inventory results by zone and datasets used estimates of total marine sediment ^{137}Cs inventories were found for this study only (n = 18) and by including datasets from Otasaka and Kato (2014) and Kusakabe et al. (2013) that were adjusted by zone based on calculated average percent inventories observed below 3 to 10 cm. See Table 3a for group numbers.

		This Study (1)			(1) & (2) & (3)			(1) & (2) & (4)		
	Zone	Mean ^{137}Cs (Bq m^{-2})	Total ^{137}Cs TBq	% of Total TBq	Mean ^{137}Cs (Bq m^{-2})	Total ^{137}Cs TBq	% of Total TBq	Mean ^{137}Cs (Bq m^{-2})	Total ^{137}Cs TBq	% of Total TBq
OZ		170 ± 160	5 ± 5	5.5 %	160 ± 120	5 ± 4	4.8 %	160 ± 120	5 ± 4	3.9 %
MCZ		1000 ± 1100	17 ± 17	17.6 %	1200 ± 1000	19 ± 16	18.3 %	1200 ± 1000	19 ± 16	14.8 %
SCZ		16 000 ± 13 000	52 ± 45	54.0 %	13 000 ± 6800	44 ± 22	42.3 %	13 000 ± 8700	42 ± 29	33 %
NCZ	Greater Area 3 km radius	4500 ± 2100	21 ± 10	21.8 %	7300 ± 5100	35 ± 24	33.6 %	13 000 ± 11 000	61 ± 52	47.5 %
		73 000	1	1.1 %	73 000	1	1.0 %	73 000	1	0.8 %
Total		100 ± 50 TBq			100 ± 40 TBq			130 ± 60 TBq		

BGD
11, 7235–7271, 2014

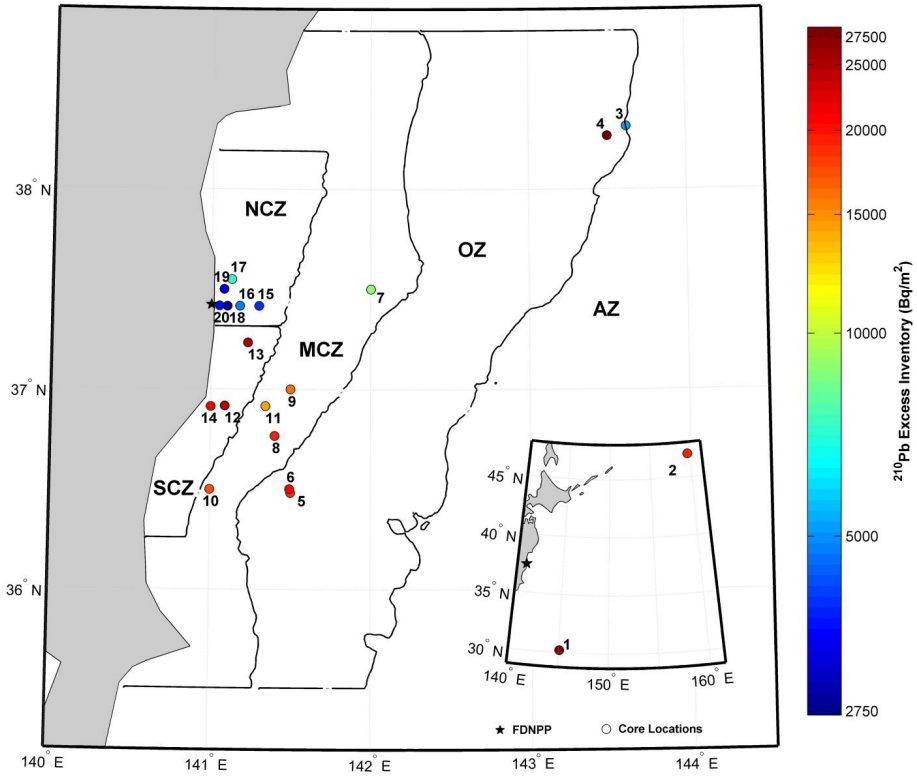

Figure 1. Core locations with $^{210}Pb_{ex}$ inventories. Larger map: contains core locations 3 to 20 and the northern coastal (NCZ), southern coastal (SCZ), mid-coastal (MCZ), offshore (OZ), and abyssal (AZ) zones. Lower right: shows core locations 1 and 2. Some of the reported values may underestimate total inventories at the locations where $^{210}Pb_{ex}$ continues to the core bottom (Fig. 2).

BGD
11, 7235–7271, 2014

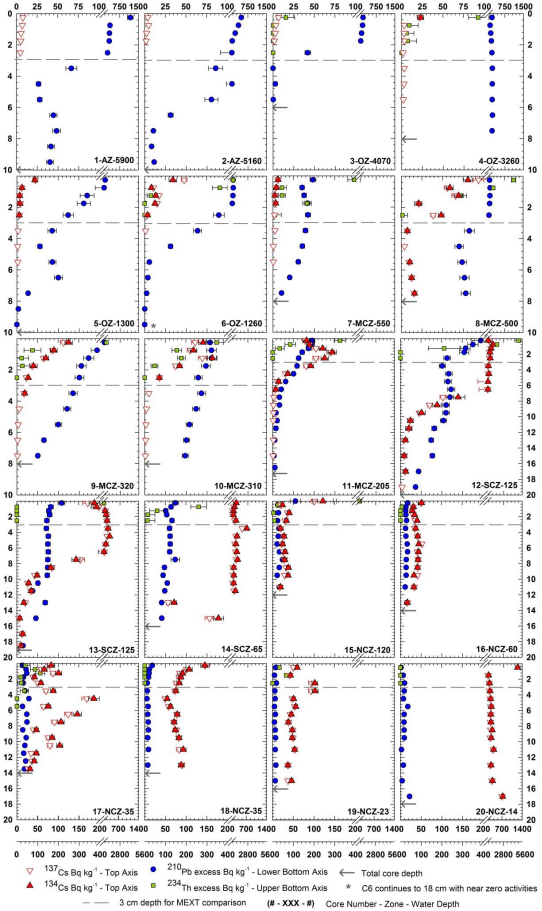

Figure 2. Sediment activity profiles in Bq kg^{-1} for ^{134}Cs, ^{137}Cs, ^{210}Pb$_{ex}$, and ^{234}Th$_{ex}$.

BGD
11, 7235–7271, 2014

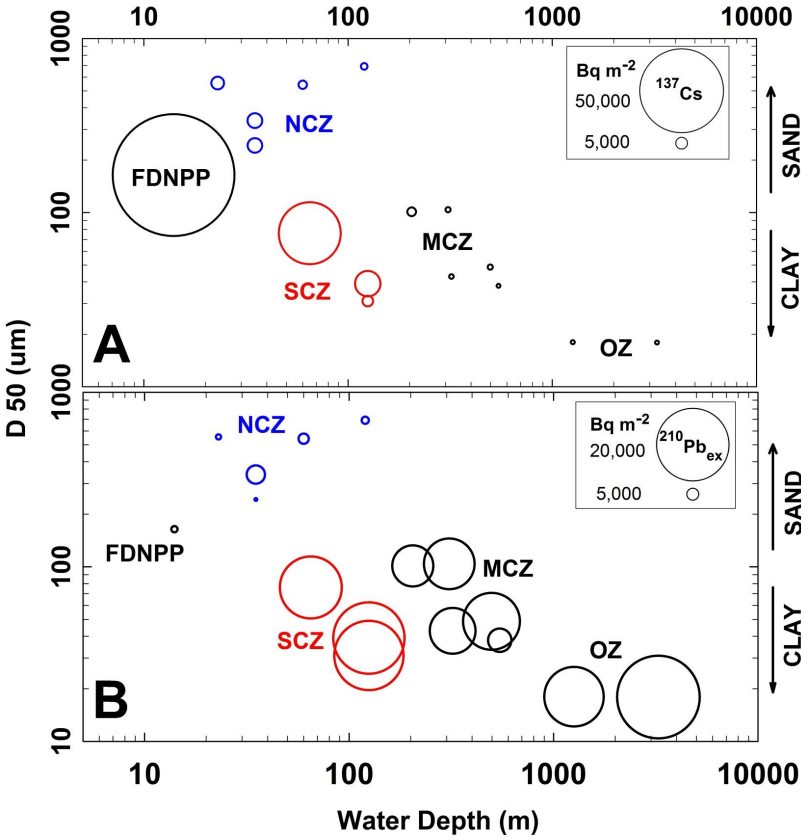

Figure 3. ^{134}Cs and $^{210}Pb_{ex}$ inventories relative to water depth and D50. Grain size distribution is shown for 16 of the 20 cores, including all of the NCZ, SCZ, and MCZ cores. Isotope inventories for ^{134}Cs **(A)** and $^{210}Pb_{ex}$ **(B)** show general depth trends with prominent grain size effects in the NCZ and SCZ.

BGD
11, 7235–7271, 2014

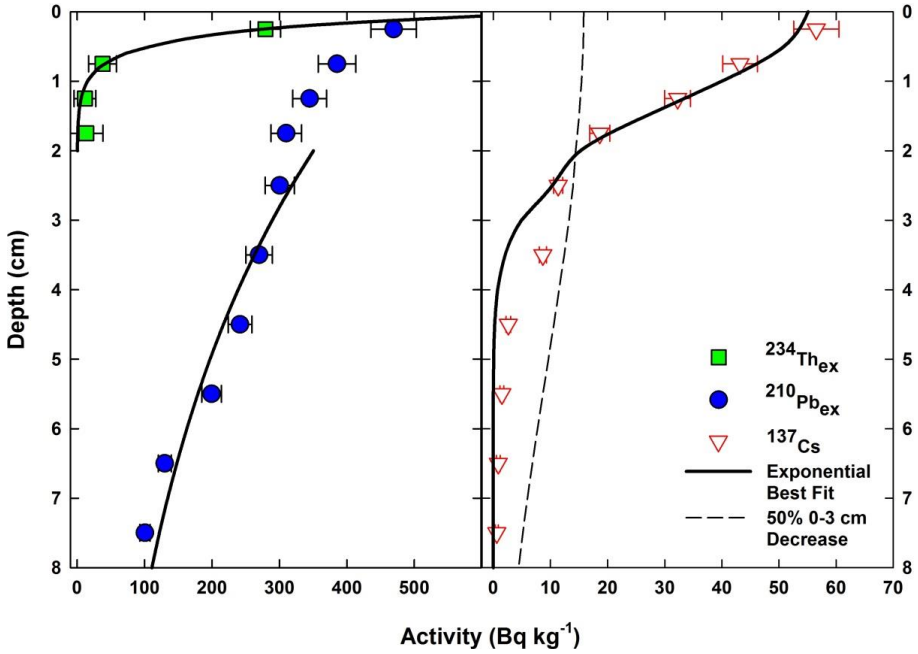

Figure 4. Example model best fit regressions for $^{210}Pb_{ex}$, $^{234}Th_{ex}$, and ^{137}Cs. for core 9. Mixing rates derived from the $^{210}Pb_{ex}$, $^{234}Th_{ex}$ profiles in the left panel were used in the cesium pulse model for the right panel. In general, the model similarly fit the profiles from the MCZ, OZ, and AZ. Model fits for the SCZ and NCZ were less successful due to almost vertical profiles for some cores.

BGD
11, 7235–7271, 2014

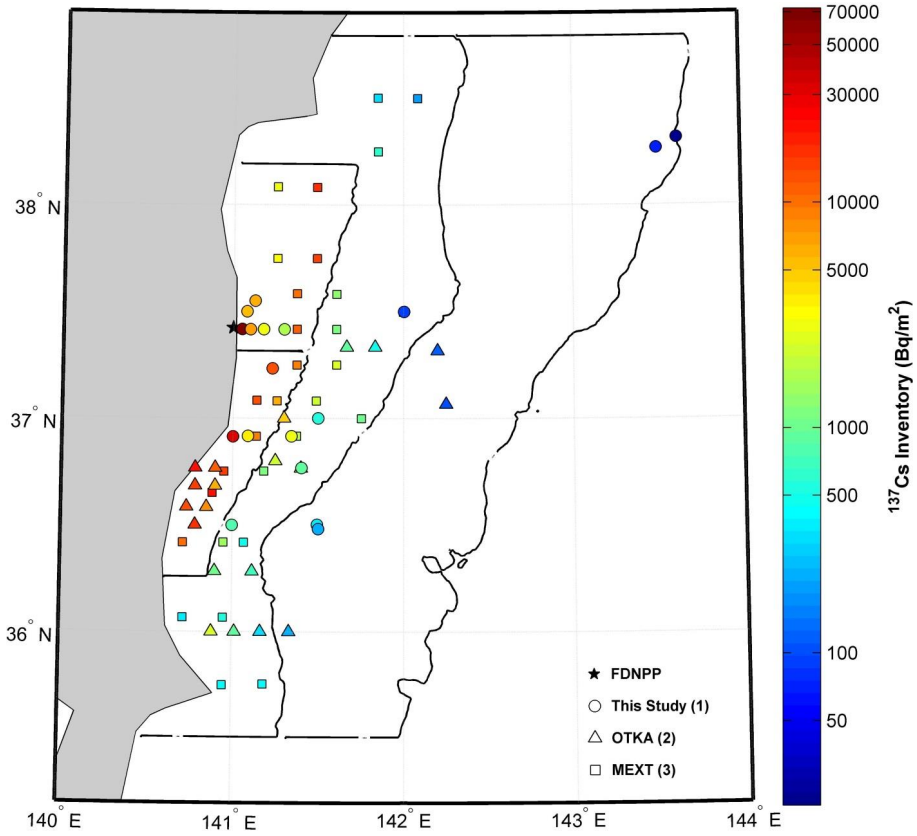

Figure 5. A compilation of sediment ^{137}Cs inventories from the coastal region around Japan, Japan Fukushima. Core inventories from this study are shown as measured from May 2012 to September 2013. MEXT cores from February 2012 (Kusakabe et al., 2013) and OTKA samples from August through November of 2011 (Otosaka and Kato, 2014) were adjusted as necessary by zone to include estimated inventories deeper than 3 cm and 10 cm, respectively (Sect. 3.5).

BGD
11, 7235–7271, 2014

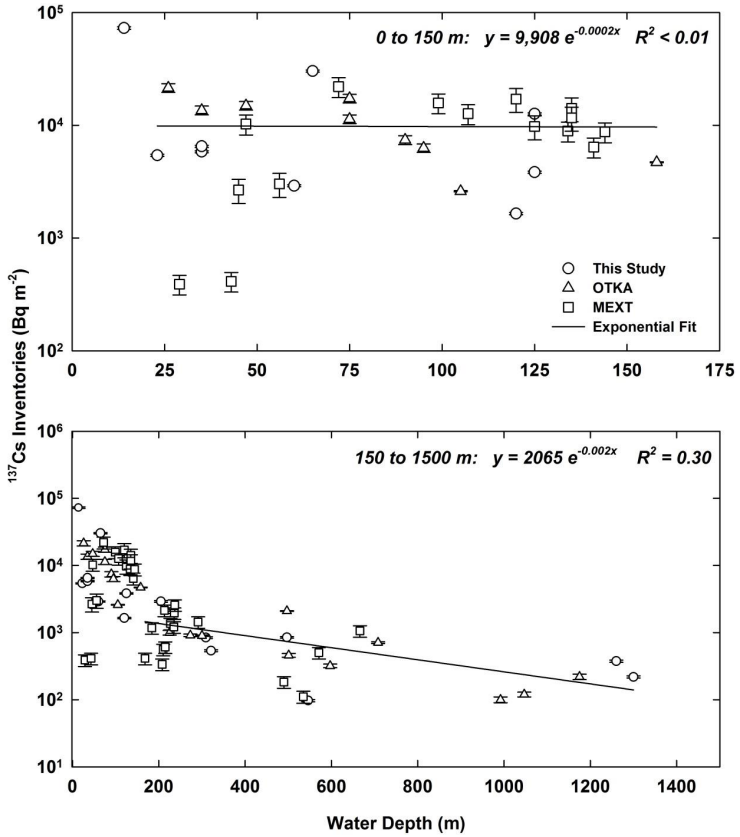

Figure 6. Spatial variations in ^{137}Cs sediment inventories with water depth. The measured and adjusted inventories from Fig. 5 are plotted against water depth. The upper figure shows the exponential regression for core inventories from 0 to 150 m, excluding core 20. The lower figure shows all inventories and the regression for cores located from 150 to 1500 m.

BGD
11, 7235–7271, 2014